Remodeling of the Connective Tissue Microarchitecture of the Lamina Cribrosa in Early Experimental Glaucoma

Michael D. Roberts,[1] *Vicente Grau,*[2] *Jonathan Grimm,*[3] *Juan Reynaud,*[3] *Anthony J. Bellezza,*[4] *Claude F. Burgoyne,*[3] *and J. Crawford Downs*[1]

Purpose. To characterize the trabeculated connective tissue microarchitecture of the lamina cribrosa (LC) in terms of total connective tissue volume (CTV), connective tissue volume fraction (CTVF), predominant beam orientation, and material anisotropy in monkeys with early experimental glaucoma (EG).

Methods. The optic nerve heads from three monkeys with unilateral EG and four bilaterally normal monkeys were three dimensionally reconstructed from tissues perfusion fixed at an intraocular pressure of 10 mm Hg. A three-dimensional segmentation algorithm was used to extract a binary, voxel-based representation of the porous LC connective tissue microstructure that was regionalized into 45 subvolumes, and the following quantities were calculated: total CTV within the LC, mean and regional CTVF, regional predominant beam orientation, and mean and regional material anisotropy.

Results. Regional variation within the laminar microstructure was considerable within the normal eyes of all monkeys. The laminar connective tissue was generally most dense in the central and superior regions for the paired normal eyes, and laminar beams were radially oriented at the periphery for all eyes considered. CTV increased substantially in EG eyes compared with contralateral normal eyes (82%, 44%, 45% increases; $P < 0.05$), but average CTVF changed little (−7%, 1%, and −2% in the EG eyes). There were more laminar beams through the thickness of the LC in the EG eyes than in the normal controls (46%, 18%, 17% increases).

Conclusions. The substantial increase in laminar CTV with little change in CTVF suggests that significant alterations in connective and nonconnective tissue components in the laminar region occur in the early stages of glaucomatous damage. (*Invest Ophthalmol Vis Sci.* 2009;50:681–690) DOI:10.1167/iovs.08-1792

From the [1]Ocular Biomechanics Laboratory and [3]Optic Nerve Head Research Laboratory, Devers Eye Institute, Legacy Health System, Portland, Oregon; [2]Department of Engineering Science, Wolfson Medical Vision Laboratory, University of Oxford, Oxford, United Kingdom; and [4]Third Eye Diagnostics, Inc., Bethlehem, Pennsylvania.

Supported in part by United States Public Health System Grants R01EY011610 (CFB) from the National Eye Institute, National Institutes of Health, Bethesda, Maryland; and grants from the American Health Assistance Foundation, Rockville, Maryland (CFB), and from The Whitaker Foundation, Arlington, Virginia (CFB).

Submitted for publication January 24, 2008; revised August 1 and September 5, 2008; accepted December 4, 2008.

Disclosure: **M.D. Roberts**, None; **V. Grau**, None; **J. Grimm**, None; **J. Reynaud**, None; **A.J. Bellezza**, None; **C.F. Burgoyne**, None; **J.C. Downs**, None

The publication costs of this article were defrayed in part by page charge payment. This article must therefore be marked "*advertisement*" in accordance with 18 U.S.C. §1734 solely to indicate this fact.

Corresponding author: J. Crawford Downs, Ocular Biomechanics Laboratory, Devers Eye Institute, 1225 NE 2nd Avenue, Portland OR 97232; cdowns@deverseye.org.

A biomechanical paradigm for the development and progression of glaucoma has been proposed that posits that the load-bearing tissues of the lamina cribrosa (LC), peripapillary sclera, and sclera are central to the underlying pathogenesis of the disease and that the manner in which they bear and respond to load is an important component of susceptibility to glaucoma.[1,2] In this paradigm, the mechanical stress and strain borne by the load-bearing tissues of the posterior pole are of special interest because they link the tissue-level mechanical environment of the optic nerve head (ONH) to the intraocular pressure (IOP) in the eye. Thus, characterization of the geometric and material properties of the connective tissue structures in the LC is a necessary step for the quantification of tissue level changes caused by experimental perturbation of IOP and for the development of mathematical models to describe the mechanical environment to which the tissues are exposed.

The LC has been implicated as the primary site of axonal damage in glaucoma, with disruption of axoplasmic transport, impaired blood flow, and mechanically mediated tissue remodeling proposed as possible underlying etiological mechanisms.[2–6] Using the monkey model of experimental glaucoma (EG) and standard two-dimensional (2D) histology, we have previously shown that permanent posterior deformation and thickening of the LC occurs soon after the induction of chronic elevated IOP.[7] More recently, we developed a three-dimensional (3D) histomorphometric technique to quantify various aspects of ONH anatomy and structure.[8–10] We have used this technique to demonstrate significant morphologic changes in the neural canal, subarachnoid space, LC, peripapillary sclera, and prelaminar neural tissues in EG monkey eyes. These studies demonstrate that changes in connective tissue occur at the earliest stages of glaucomatous damage and provide supporting evidence for a biomechanical basis of the disease.

The arrangement of the connective tissue of the LC bears many morphologic similarities to porous, open-celled structures such as engineered foams and trabecular bone. Such materials are typically inhomogeneous and anisotropic, characteristics that can have a profound influence on their structural load-bearing and directional stiffness characteristics. Previous research has shown that pore and beam size vary regionally in the LC, and it has been suggested that this nonuniformity may be related to the patterns of damage and visual impairment associated with glaucomatous vision loss.[11–13]

The present report describes a quantification technique to characterize the complex architecture of the LC connective tissue network in ONH tissues harvested after death. We characterize the normal and EG eyes from cynomolgus monkeys described in our previous reports[8–10] along with a group of nontreated bilaterally normal eyes from rhesus monkeys. Our technique defines the laminar space as a two-phase material consisting of connective or neural tissue and uses a volumetric approach to regionally characterize the amount of connective tissue in contiguous regions of the LC. We also adopt the concept of *fabric* to describe the textural anisotropy that results from the microarchitectural arrangement of pores and

beams within the LC. The mean intercept length (MIL) method is used to locally characterize fabric in terms of the predominant orientation of the lamina cribrosa beams and the relative strength of that orientation. The MIL method has been used in other fields to characterize and compare materials and tissues with complex microstructures.[14–17]

Although this approach is useful by itself as a microstructural characterization technique for the fenestrated connective tissue network of the LC, it also serves as the basis for formulating a mathematical description of the regional mechanical behavior of this complex load-bearing structure. Thus, in this report, we have cast these microarchitectural quantities in a manner such that they may be readily incorporated into biomechanical finite element models of the ONH so as to impart the effects of LC connective tissue inhomogeneity, anisotropy, and predominant directional stiffness on load transmission and deformation. The exploitation of this LC characterization within a finite element-based framework to model the stress and strain within the peripapillary sclera and ONH will be the subject of a future report.

Materials and Methods

Animals

All animals were treated in accordance with the ARVO Statement for the Use of Animals in Ophthalmic and Vision Research. Three male cynomolgus monkeys (monkeys 1, 2, 3), approximately 8 years of age, were used for the EG portion of this study (Table 1 of our previous report[18]). In addition, four untreated rhesus monkeys (monkeys 4, 5, 6, 7 [three females aged 8–10 years and one male age 2 years]) were used to assess the physiological intereye difference in LC morphology and microarchitecture in pairs of eyes from bilaterally normal monkeys.

Early Experimental Glaucoma

Early experimental glaucoma was induced in one eye of the EG monkeys by photocoagulation of the trabecular meshwork, resulting in chronic but moderate IOP elevations. This methodology and specific information about these three monkeys are included in our previous reports.[8–10,18] In this work, EG was defined as the earliest confirmed change in ONH surface position or compliance, as measured by confocal scanning laser tomography (CSLT). A brief summary of the duration and magnitude of moderate IOP elevations for each EG monkey is as follows: monkeys 2 and 3 were killed 3 weeks and monkey 1 was killed 6 weeks after CSLT-detected ONH surface position or compliance change. In monkeys 1 and 2, IOP elevations were moderate; only one measurement was higher than 30 mm Hg. In monkey 3, elevated IOP was not detected, though there was a confirmed ONH surface change (Table 1, Fig. 1 of our previous publication[18]). Axon loss in the EG eyes of these three monkeys averaged 16%, 30%, and 19% in monkeys 1, 2, and 3, respectively, which achieved statistical significance in all cases.[9]

Three-Dimensional Reconstruction and Delineation of ONH and Peripapillary Sclera

Paraffin-embedded tissue samples containing the ONH and peripapillary sclera were three dimensionally reconstructed using a serial-sectioning technique described previously.[18] Briefly, a microtome-based system has been developed wherein stain is manually applied to the newly cut blockface of an embedded tissue sample during sectioning. The stain is a 1:1 volumetric mixture of Ponceau S and acid fuchsin, which allows visualization of exposed connective tissue on the blockface surface but does not stain nonconnective tissue or glial structures. High-resolution images are consecutively acquired at 3-μm intervals, stacked, and aligned to produce volumetric histologic datasets (voxel resolution of 2.5 $\times$ 2.5 $\times$ 3.0 μm) suitable for visualization and morphometric analysis. Since its introduction, the system has been upgraded so that a higher voxel resolution of 1.5 $\times$ 1.5 $\times$ 1.5 μm is captured. In the present work, the ONHs from the EG monkey were reconstructed at a 2.5 $\times$ 2.5 $\times$ 3.0-μm resolution, and the ONHs from the bilaterally normal monkeys were reconstructed at a 1.5 $\times$ 1.5 $\times$ 1.5-μm voxel resolution. All other treatments were identical.

Isolation and Segmentation of the Lamina Cribrosa from the 3D ONH Reconstructions

Within each 3D ONH reconstruction, custom software was used to interactively delineate various anatomic landmarks and surfaces in 3D space at 40 consecutive, radial (4.5° interval) sections.[8] In the present work, this system was used to delineate surface points corresponding to the neural canal wall and the anterior and posterior surfaces of the LC and peripapillary sclera. The delineated points for the anterior and posterior sclera and LC surfaces were fit with B-spline surfaces using custom software routines (MATLAB; The Mathworks, Natick, MA), resampled at a higher point density, and imported into a computer-aided design package (Geomagic Studio 8; Raindrop Geomagic, Research Triangle Park, NC) for additional processing. A Boolean intersection between the anterior and posterior scleral-LC surfaces and the neural canal wall surface was performed to define the boundaries of a volume enclosing the LC space (Figs. 1A–C). This volume definition was used as a mask to identify all voxels within each 3D ONH reconstruction corresponding to the LC volume.

We have developed a custom 3D segmentation algorithm specifically designed to classify voxels in the lamina of our 3D ONH reconstructions as either connective or nonconnective tissue.[19] This 3D anisotropic Markov random-field algorithm uses measures of image anisotropy and local principal orientations to ensure that the inherent trabecular connectivity of the LC microarchitecture is maintained, even in the presence of image noise, nonuniform staining, and discontinuities caused by the presence of internal capillaries. The algorithm includes preprocessing steps that correct for nonuniform illumination through the serial image stack and enhance the contrast between connective and nonconnective tissues by transforming the acquired images into LUV color space. A third preprocessing step is used to identify and eliminate pigmentation not associated with connective tissue that was present in several of the eyes from the bilaterally normal monkeys. The 3D segmentation algorithm operates on the preprocessed U-channel images and results in a binary volume identifying voxels in the lamina cribrosa as either connective or nonconnective tissue. Note that the segmentation algorithm fills in the capillary space within the laminar beams by classifying each capillary lumen as connective tissue. The final segmented 3D binary volumes form the basis for the visualization and quantification procedures used in this report.

Regionalization of the Segmented LC Volume

The LC volume was discretized into 45 subvolumes using the volumetric mesh generation capabilities of a finite element preprocessing and postprocessing software package (PATRAN; MSC Software, Santa Ana, CA), with each subvolume represented by an isoparametric quadratic hexahedral element.[20] The element sizes were selected to ensure that an adequate sampling volume was used to estimate the predominant LC beam orientation and anisotropy.[21] The element subvolumes encompassed an average of 340,000 and 1.3 million voxels per element in the low- and high-resolution reconstructions, respectively. Figure 1D shows an example of the laminar regionalization scheme, along with a representative element and its associated segmented, voxel-based connective tissue microstructure.

Connective Tissue Volume Fraction and Fabric Measurement

For each elemental subvolume, the isoparametric element definition was used to identify voxels lying on or within the given element. The total number of voxels within each element was summed, with each identified voxel tagged as either connective or neural tissue. The following quantities were calculated and converted to cubic micrometers: total CTV in the LC, CTV within each element, connective tissue volume fraction (CTVF) for each element (ratio of CTV to the entire

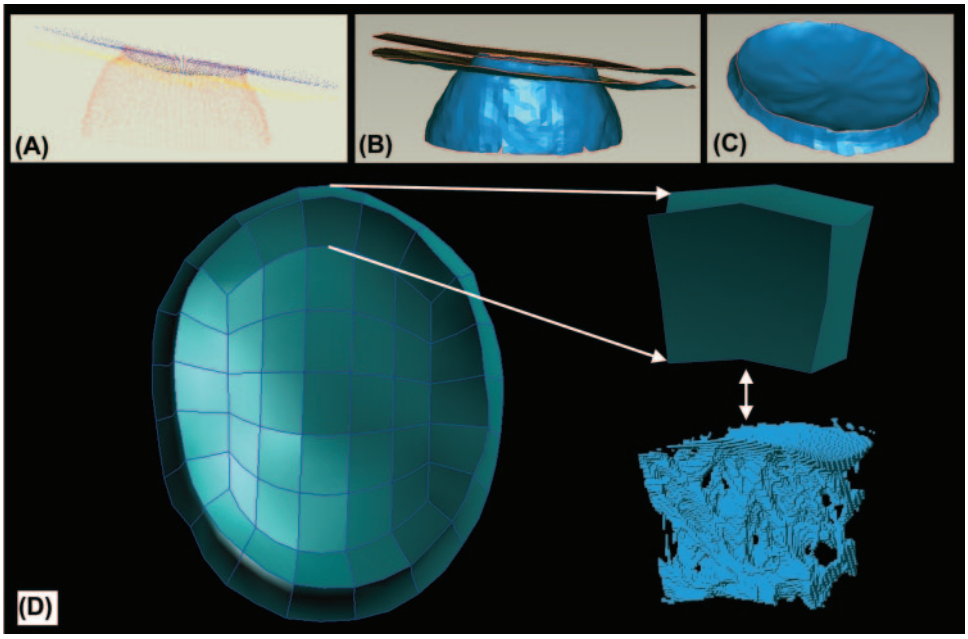

FIGURE 1. Isolation and regionalization of the lamina cribrosa volume in each 3D ONH reconstruction. (**A**) The delineated landmark points corresponding to the anterior LC and peripapillary scleral surface (*blue*), neural canal (*red*), and posterior LC and peripapillary scleral surface (*yellow*) are used to generate three distinct surfaces (**B**). (**C**) The intersection and union of these surfaces are used to isolate a surface boundary that encloses the LC volume. (**D**) The LC volume is discretized into 45 volumetric subregions using quadratic hexahedral finite elements. Each elemental subvolume contains the binary, segmented LC connective tissue voxels derived from the original 3D reconstruction data.

element volume), and mean CTVF across the entire LC volume. Total CTV for each eye was normalized relative to the EG eye in the EG monkeys or the smaller of the two eyes in the bilaterally normal monkeys, and a paired *t*-test was used to assess the effect of treatment on this measure. No other statistical tests were used because of the nonuniformity inherent in the elemental subvolume sampling in the regional measures.

The fabric within each elemental subvolume was characterized by calculating the predominant beam orientation and anisotropy using the MIL method.[15,16,22,23] A brief illustration of the MIL-based quantification of fabric using a 2D image and an oriented ellipse is shown in Figure 2A–C. In 3D, the MIL characterization method results in an *ellipsoid*, which may be represented mathematically as second-rank tensor, M.[24] An algebraically modified fabric tensor, H, was calculated as the inverse square root of M; the advantage of this representation is that the eigenvalues of H correspond to the three principal radii of the ellipsoidal representation and reflect the degree of anisotropy of the microstructure, and the eigenvectors define a local coordinate system reflecting the principal directions along which the structural components are oriented.[22] We adopted the convention that the eigenvalues of H (H_1, H_2, and H_3) were ordered as $H_1 > H_2 > H_3$ and normalized such that $H_1 + H_2 + H_3 = 1$ to provide a measure of relative anisotropy in each of the three principal directions and to facilitate the comparison of fabric between different samples. To this end, we also calculated the *anisotropy ratio* as the ratio between the maximum and minimum eigenvalues to characterize the relative degree of material orientation within a given element. Implementation of the MIL-based fabric calculations was carried out using custom programs designed around the Visualization Toolkit (Kitware, Troy, NY). An example of an elemental subvolume of laminar connective tissue analyzed according to this 3D method is shown in Figure 2D–F.

Figure 3 shows the regional mapping of CTVF and the predominant laminar beam orientation measures colocalized to the 3D reconstruction of the LC from a representative normal monkey eye (right eye of monkey 6). This figure demonstrates that the reported measures faithfully represent the character of the underlying LC microarchitecture.

Evaluation of the Nature of Laminar Connective Tissue Remodeling

An analysis was performed post hoc to estimate the number of laminar beams aligned in the plane of the LC of each eye to determine whether the additions in CTV seen in EG eyes (see Results) were caused by thickening of the original laminar beams or the addition of new laminar beams. The MIL program was modified to cast probe lines through each elemental subvolume in the anterior-posterior direction only and to determine the average number of connective-nonconnective tissue transitions per number of rays cast. To ensure that only probe lines that traversed the full thickness of the LC were included in the analysis, intercept data from the shortest 20% of rays were discarded for each element. This measurement provides an estimate of the average number of laminar beams through the thickness of the LC in each eye.

RESULTS

3D Reconstructions of EG Eyes

LC connective tissue reconstructions for three pairs of eyes for which histomorphometric data have been reported[8–10,18] are shown in Figure 4. These reconstructions highlight the degree of individual-specific variation in overall shape that occurs naturally within the monkey LC and reveal a consistent EG treatment effect on LC morphology. The treatment effects shown in this figure greatly exceed the physiological intereye differences in bilaterally normal monkeys.[25] In particular, sectional views through the superior-inferior and nasal-temporal directions facilitate comparisons of LC shape that are difficult to convey in the en face views. For instance, comparison of the three normal eye LC reconstructions showed that individual variation in LC geometry was apparent in LC position and in anterior-posterior thickness. Reconstructions and sectional views highlight the substantial amount of posterior cupping in the connective tissue of the EG eyes compared with their contralateral normal controls (average of 98 μm and 93% deeper in the EG eyes). Similarly, there was a pronounced anterior-posterior thickening of the LC in the EG eyes (average of 37 μm and 36% thicker in the EG eyes vs. their normal controls). Thus, visualization of the segmented volumes qualitatively confirms the previously reported data quantifying the histomorphometric changes in laminar position and thickness in EG for these animals.

LC Connective Tissue Characterization

Changes in Total LC CTV Caused by EG. The total CTVs in the LC increased significantly by 82%, 44%, and 42% in the EG eyes of monkeys 1, 2, and 3, respectively, compared with their contralateral normal controls (Fig. 5; $P < 0.05$). In con-

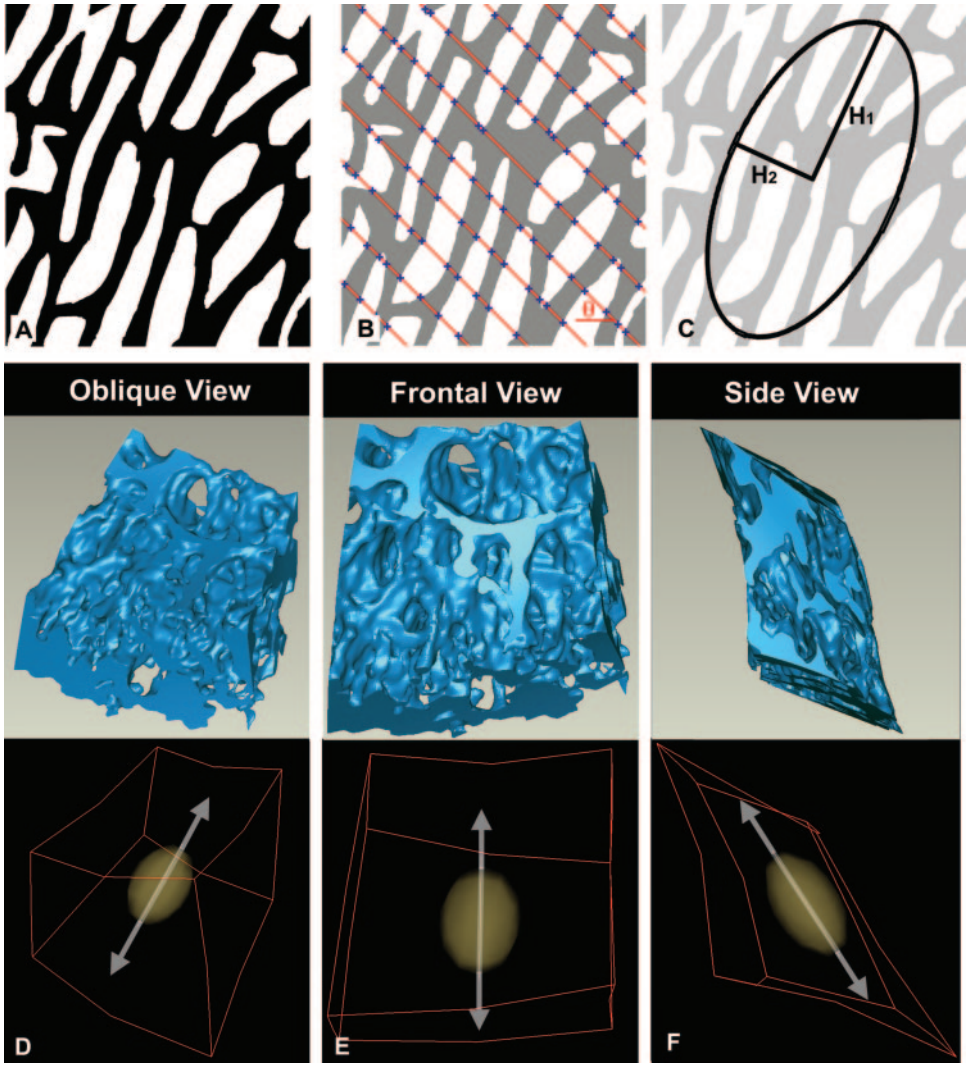

FIGURE 2. Fabric representation of 2D and 3D structures using mean intercept length. Predominant laminar beam orientation is obtained from the binary, segmented, LC volume by extending the 2D mean-intercept-length (MIL) algorithm presented in (**A**) to (**C**) into three dimensions. (**A**) A 2D segmented image of an oriented microstructure. (**B**) Probe lines (*red*) are passed through the microstructure at different angles, θ, and the number of intercepts with the microstructure (*blue crosses*) are calculated for each probing angle. When algebraically manipulated and plotted in polar coordinates, the angular MIL values form an ellipse (**C**), where the direction of the major axis (H_1) reflects the predominant orientation of the beams in (**A**) and the ratio of the ellipse radii (H_1/H_2) indicates the strength of the predominant orientation of the microstructure (i.e., degree of anisotropy). When this method is extended to 3D and performed in the segmented LC volume, an oriented ellipsoid coinciding with the predominant LC beam orientation in that region is produced. (**D–F**) Three different views of the LC microarchitecture from a single elemental region and its corresponding MIL ellipsoid, with the predominant LC beam orientation direction highlighted (*arrow*). In subsequent figures, these arrows are color coded to indicate the strength of the predominant orientation of the laminar beams (degree of anisotropy expressed as the ratio of the lengths of the major and minor ellipsoid axes).

trast, as also shown in Figure 5, bilateral normal monkeys showed no significant differences in total laminar CTV (12%, 4%, 12%, 14% differences between contralateral eyes in monkeys 4, 5, 6, 7, respectively; Fig. 5; $P = 0.14$).

When comparing the number of laminar beam intercepts in the anterior-posterior direction in all eyes, the mean number of laminar beams through the thickness of the LC was greater in the EG eyes (46%, 18%, and 17% higher than in their contralateral normal eyes for monkeys 1, 2, and 3, respectively). These treatment differences exceeded the physiological differences seen in the bilaterally normal monkeys (7%, 5%, 7%, and 15% differences between contralateral normal eyes in monkeys 4, 5, 6, and 7, respectively).

Regional Variations in LC Connective Tissue Morphology in Normal Eyes. To quantify regional variation of the microstructure in each LC reconstruction, the local CTVF, predominant beam orientation, and degree of anisotropy were assessed for 45 elemental subvolumes in both eyes of four bilaterally normal monkeys (monkeys 4–7) and are rendered in Figure 6. The background grayscale values in Figure 6 indicate that regional CTVF exhibits considerable regional variation within normal eyes and between monkeys but show similar patterns in contralateral eyes from the same monkey. Note that there are distinct regions in which the CTVF is markedly higher, particularly in areas encompassing the central vascular trunk, where the connective tissue structure is robust (Figs. 3, 5). Conversely, all eyes exhibit regions of low CTVF near the periphery of the LC. In broad terms, the CTVF maps show that the lamina is most robust centrally and superiorly, with the most porous regions occurring variably in the inferior, nasal, and temporal periphery.

The oriented colored arrows in Figure 6 indicate the predominant LC beam orientation and the relative degree of anisotropy for each elemental region. Note that the laminar beams in the regions adjacent to the neural canal wall have a strong radial orientation. This radial orientation at the LC periphery likely reflects the tethering and insertion of the LC beams into the peripapillary sclera. In contrast, beam directionality in the central LC is more diverse across all eyes. For all eyes, the primary orientation of the laminar beams is generally within the plane of the LC itself. This is evident in the arrow orientation in Figure 6, in which no arrows are pointing in the anterior-posterior direction (i.e., none appear to be "on end").

The local degree of anisotropy, expressed as a color-coding of the orientation arrows in Figure 6, also exhibited considerable regional variation in all eyes. In general, the laminar beams tended to be less oriented in the periphery of the LC and more oriented in the central region.

Regional Variations in LC Connective Tissue Morphology Caused by EG. Figure 7 shows only modest overall differences in mean CTVF, predominant beam orientation, and anisotropy ratio between contralateral normal and EG eyes. These differences do not exceed the physiological intereye variation between eyes from bilaterally normal monkeys seen

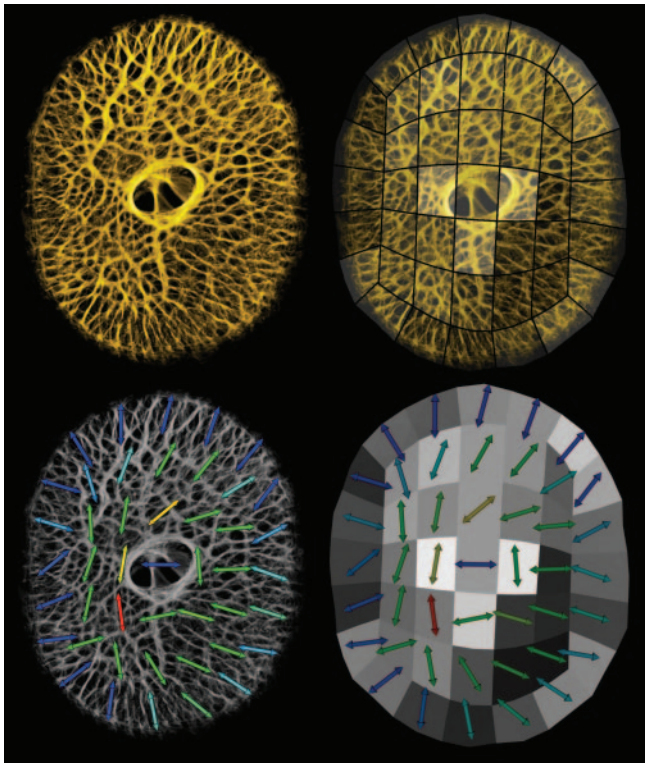

FIGURE 3. A 2D projection of a representative 3D reconstruction of the lamina cribrosa from a normal monkey eye (*top left*) showing the regional diversity of the connective tissue microarchitecture colocalized with the reported measures. The regionalization scheme (based on volumetric finite elements; *top right*) with the variation in CTVF highlighted as a translucent overlay (lighter areas indicate higher CTVF). Darker areas directly correspond to areas in the underlying microarchitecture that contain proportionally less laminar connective tissue. Regional predominant laminar beam orientations are shown as colored *arrows* (*bottom left*), which clearly capture the directional character of the underlying laminar microstructure. When these measures are combined with anisotropy, the resultant maps (*bottom right*) accurately quantify the regional character of the laminar microarchitecture, in which the arrow direction indicates the predominant laminar beam orientation in each region, the arrow color coding indicates the strength of that laminar beam directionality (the degree of anisotropy), and the background grayscale shading reflects CTVF.

in Figure 6. Additional descriptive data on the distributions of the 45 regional measures of CTVF and the anisotropy ratio within each eye of all monkeys (Figs. 8 and 9) confirm this finding.

DISCUSSION

In this report, we have used voxel counting within 3D ONH reconstructions to show that the amount of connective tissue within the LC was significantly increased at the earliest detectable stage of glaucomatous damage in three monkeys with unilateral chronic IOP elevations. In addition, we used MIL-based fabric measurements to quantify the considerable spatial variation in microarchitecture for normal and EG eyes as manifest in local CTVF, predominant LC beam orientation, and material anisotropy. These microstructure characterization maps (Figs. 6, 7) represent a quantitative regional description of the connective tissue morphology associated with each of the 3D laminar reconstructions from the three EG monkeys presented in Figure 4 and those from four bilaterally normal monkeys. In addition to quantifying regional LC microarchitecture, these measures form the basis for describing the regional mechanical stiffness of the LC connective tissues that will be used in future biomechanical models of the ONH.

Volumetric rendering and sectioning of the 3D LC reconstructions of the EG monkey eyes illustrate an increase in laminar thickness and a significant posterior displacement of the anterior LC surface caused by EG. These phenomena were quantified for these same animals in a previous report using a related technique.[10] We have proposed that posterior displacement of the anterior LC surface underlies "true glaucomatous cupping" and is distinct from cupping induced by loss of the prelaminar neural tissues.[9] The presence of glaucomatous cupping at the earliest detectable stage of the disease reinforces the notion that perturbation of LC connective tissue underlies and mediates subsequent glaucomatous progression. Indeed, we expect that the increase in LC thickness observed at this early stage of damage is a transient phenomenon that will be

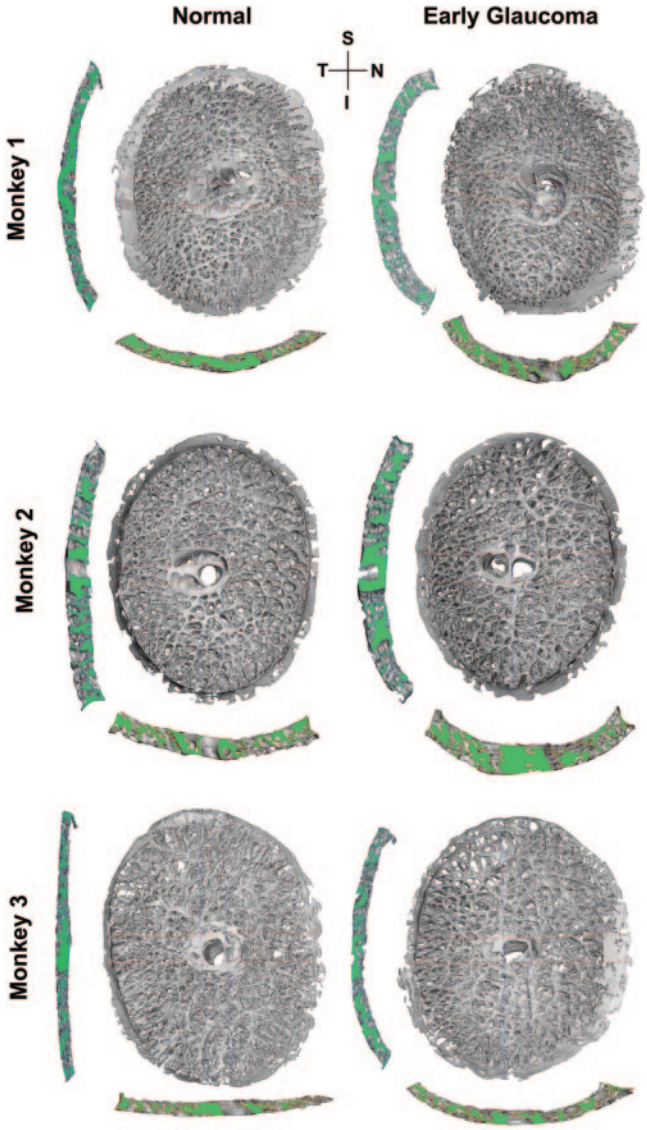

FIGURE 4. 3D reconstructions of the LC connective tissues of three pairs of monkey eyes with one eye of each pair having early EG (note that all eyes are in OD configuration). Central superior-inferior and nasal-temporal sections from the LC of each eye are shown to the *left* and *bottom* of each 3D LC reconstruction, respectively. Note the regional differences in LC morphology present within and between eyes as well as the changes in LC curvature and thickness induced by EG (reported previously by Yang et al.[10]). S, superior; I, inferior; N, nasal; T, temporal.

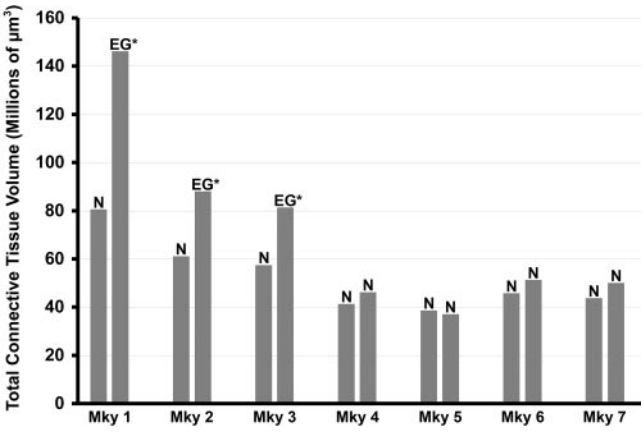

FIGURE 5. Total connective tissue volume in the LC of both eyes of all monkeys. Connective tissue volume is remarkably similar between contralateral eyes of the bilaterally normal monkeys (monkeys 4–7; $P = 0.14$) but is significantly higher in all three EG eyes compared with their contralateral normal controls (monkeys 1–3; $P < 0.05$). N, normal eye; EG, early glaucoma eye. $^*P < 0.05$; statistically significant difference compared with the contralateral eye.

followed by a longer term remodeling response that will eventually transform the LC into the more familiar excavated and compressed conformation characteristic of end-stage glaucoma.[26–28]

The 3D reconstructions also facilitate the visualization of the porous neural tissue space to further inform our understanding of this complex microstructure. Although it is clear from the 3D reconstructions that a great deal of anterior-posterior directionality exists in the neural tissue space (traditionally viewed as channeling through perforated plates), they also highlight the fact that there is substantial lateral interconnectivity of the neural tissue pore space within the LC itself. In other words, the microstructure is less like a set of stacked perforated plates and more like a sponge through which directed pores channel anteriorly to posteriorly, with openings and connectivity existing between adjacent pores. A similar overlap and subdivision of pores as they traverse the LC in the anterior-posterior direction has been described previously in humans.[29]

The spatial distribution of pore size and connective tissue density in the LC has been studied and reported extensively for humans and monkeys.[11–13,29–32] From these studies, a characteristic "hourglass-shaped" distribution of pore size and connective tissue density has been described, with the superior and inferior poles exhibiting greater pore space (and reduced connective tissue density) than nasal and temporal quadrants. Our results do not support this finding in monkey eyes. In the normal monkey eyes studied herein, we found that the greatest connective tissue density was located in the central and superior regions of the LC (Figs. 3, 4, 6, 7), which is at odds with the previously reported superior-inferior pattern of lower CTVF.[11–13,30,31] In addition, CTVF appeared lower at the periphery of the LC (variably present in the temporal, inferior, and nasal quadrants), where beams tended to radially tether into the neural canal wall, a finding that concurs with two studies in human eyes.[12,30]

It has been suggested that the distribution of laminar connective tissue (CTVF) may be relevant to the arcuate pattern of vision loss in clinical glaucoma.[11,28] Similarly, the spatial distribution of connective and neural tissue has been cited in connection with the axonal transport blockage associated with acute increases in IOP.[3,33] Although the CTVF patterns in these eyes are less pronounced and regular than reported previously, axon loss in the EG eyes of monkeys 1 to 3 was similarly diffuse and did not consistently show a regional pattern (see Fig. 12 in our previous report on these same monkeys[9]).

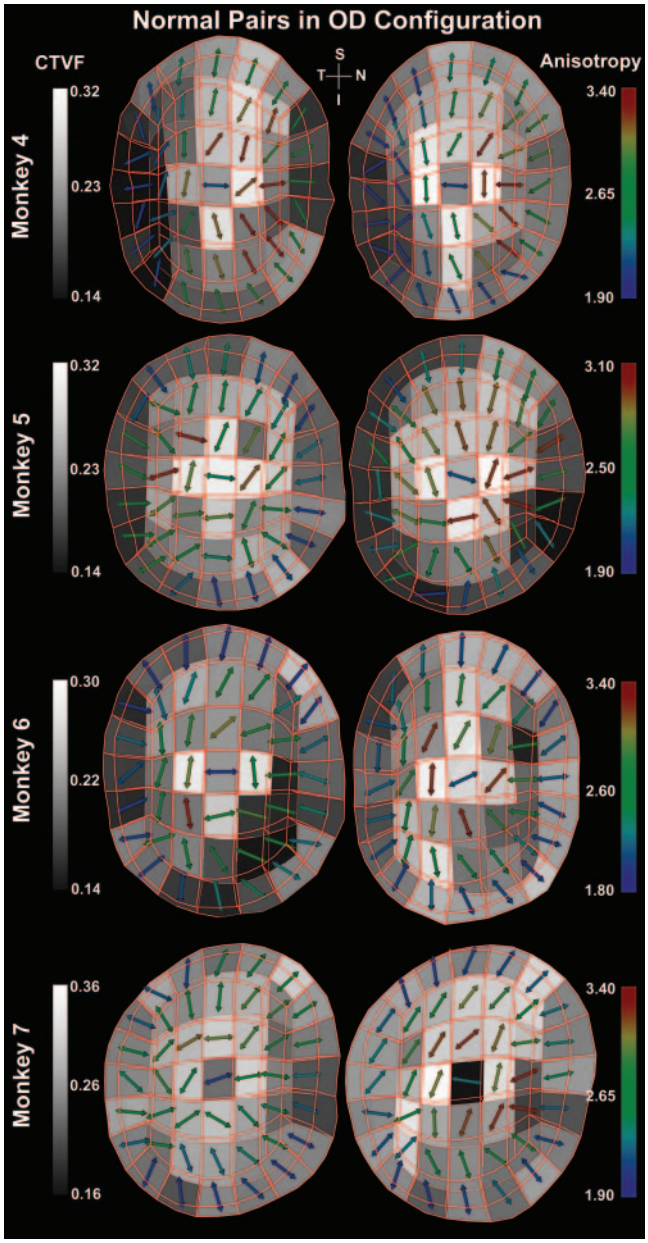

FIGURE 6. Regional connective tissue volume fraction and anisotropy ratio in the LC of four bilaterally normal monkeys (all eyes are in OD configuration). The background *grayscale* shading reflects the CTVF of the LC microarchitecture in that region. The *colored arrows* show the predominant laminar beam orientation in each region, and the *arrow color coding* indicates the strength of that laminar beam directionality (the degree of anisotropy). If the degree of anisotropy is 1.0, the laminar beams in that region are randomly oriented and show no directional predominance. Values above 1.0 indicate that the laminar beams are oriented in the direction of the arrow, and high values indicate that the beams are highly oriented in the direction of the arrow. Note that the laminar beams are principally oriented in the plane of the lamina (like threads in the fabric of a trampoline). In addition, in the periphery of the LC, the beams are primarily oriented radially to tether into the scleral canal wall. Note that the CTVF, trabecular orientation, and anisotropy patterns are remarkably similar between contralateral eyes of the same monkey but differ substantially between animals. Note also that CTVF is generally highest in the central region and lowest in the periphery.

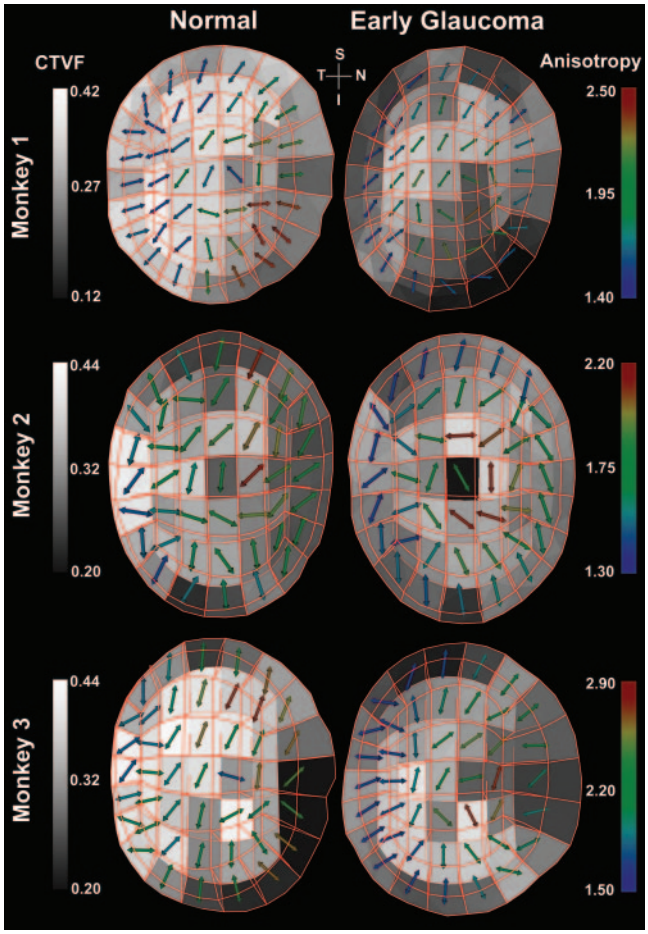

FIGURE 7. Regional connective tissue volume fraction and anisotropy ratio in the lamina cribrosa of three monkeys with EG induced in one eye (note that all eyes are in OD configuration). See Figure 6 for an explanation of the quantities depicted in these maps. Note that the CTVF, trabecular orientation, and anisotropy patterns are not as similar between the normal and EG eyes of these monkeys as seen in the contralateral normal eyes in Figure 6. The regional maps of both quantities differ substantially between animals. As seen in the normal eyes in Figure 6, CTVF is generally highest in the central region and lowest in the periphery, and laminar beam orientation is predominantly radial in the periphery.

In addition, our results contradict the higher connective tissue density at the periphery of the LC and in the nasal versus temporal regions, as reported by Radius et al. in monkeys.[13] A possible explanation for this discrepancy is that the natural curvature of the LC as a whole and the inherent directionality of the laminar beams make quantification of laminar connective tissue and pore characteristics problematic when analyzing individual 2D histologic sections, as performed in the previous study. In particular, measurements from en face histologic LC sections may be misleading because they can potentially expose greater tissue density in some regions than others during sectioning, particularly in the periphery of a curved structure such as the lamina,[31] and they are subject to additional measurement errors induced by specimen tilt relative to the sectioning plane. A distinct advantage of the 3D volumetric quantification method used in this study is that it is relatively immune to such artifactual errors common to 2D approaches.

A surprising finding in this work was that although the total amounts of connective and nonconnective tissue volume increased substantially in EG, they did so in proportions that resulted in small net changes in CTVF. It should be noted that the increase in total laminar volume is attributed to two distinct phenomena acting in concert to modify the morphology of the LC: the lamina thickens (an average of 36% thicker in the EG eyes[10]) and changes shape (the neural canal expands[8] and the LC deforms posteriorly [cupping][10]). During this reconfiguration of the LC, the connective and nonconnective tissue components appear to increase in similar proportions, raising questions about the origin of these "new" components.

We propose that two principal factors contribute to the volumetric increase of the connective and nonconnective tissue components of the LC in EG. First, the expanded connective tissue volume was caused by existing laminar beams becoming thicker and the effective recruitment of immediate retrolaminar septae into the load-bearing LC structure through thickening of their connective tissue components (both presumably occurring through connective tissue synthesis). Second, the increase in nonconnective tissue volume resulted from swollen axons (possibly because of IOP-induced axoplasmic transport blockade) and new extra-axonal nonconnective tissue (glial proliferation and hypertrophy).

Alternatively, the balanced increases in the connective and nonconnective tissue volume in EG eyes might have been driven solely by tissue edema, occurring simultaneously and in similar proportions in both tissue classes and producing the increases in LC thickness and tissue volume observed in the EG eyes. However, the ample evidence of increased glial activation, proliferation, and simultaneous connective tissue synthesis in glaucomatous eyes [6,34–38] seems to argue against a purely edematous mechanism to account for the increased component volumes observed.

Our analysis of laminar beam intercepts in the anterior-posterior direction through the LC suggests that there are, on

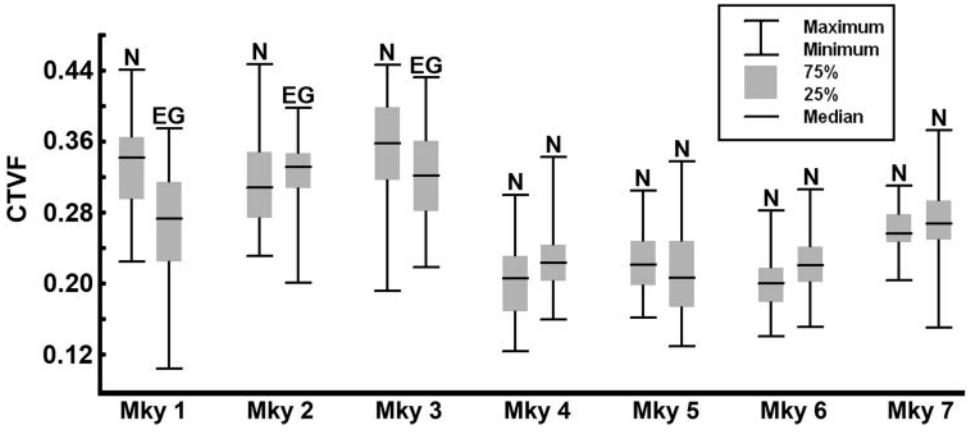

FIGURE 8. Distribution of regional connective tissue volume fraction measures in the lamina cribrosa of all monkeys (three with EG in one eye and four bilaterally normal). CTVF is remarkably similar between contralateral eyes of the bilaterally normal monkeys, and CTVF ranges overlap in all animals. With the exception of monkey 1, CTVF is similar between the EG and normal eyes in the treated monkeys. Note that the EG eye in monkey 1 also exhibited the most change in total connective tissue volume (Fig. 3) and LC thickness and position (Fig. 4) compared with its contralateral normal control.

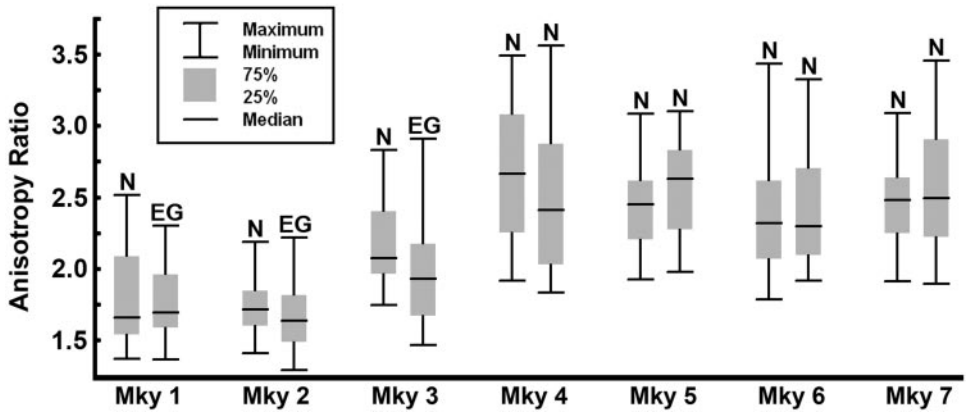

FIGURE 9. Distribution of the regional anisotropy ratio measures in each eye of all monkeys (three with EG in one eye and four bilaterally normal). The anisotropy ratio is remarkably similar between contralateral eyes of both the treated and the bilaterally normal monkeys, and the anisotropy ratio ranges overlap in all animals.

average, more connective tissue beams through the thickness of the LC in EG eyes (46%, 18%, and 17% more beams in the EG eyes than their contralateral controls in monkeys 1, 2, and 3, respectively). We propose that these so-called new laminar beams within the LC arise from the thickening of the connective tissue components of the retrolaminar septae and their recruitment into horizontally oriented, load-bearing structures that are indistinguishable by our 3D histomorphometric method from the original scleral laminar beams. We have reported preliminary laminar beam thickness data for these same three EG monkeys (Grimm J, et al. *IOVS.* 2007;48:ARVO E-Abstract 3295). Overall, while thickening and thinning of the laminar beams occur regionally in the EG eyes, these changes in beam thickness result in only small net changes in average laminar beam thickness in the EG eyes when compared with their contralateral normal controls. Combined, these data suggest that it is the addition of new laminar beams rather than the thickening of existing beams that accounts for the increased CTV seen in early EG.

In this "thickening and recruitment of retrolaminar septa" hypothesis, the overall thickening of the anterior-posterior LC boundary and increase in connective and nonconnective tissue volume in EG eyes represents a bulking up of retrolaminar septae that shifts the identifiable posterior LC boundary even more posteriorly, resulting in a net increase in effective LC thickness and volume. Although the septal microarchitecture is largely regarded as smaller connective tissue structures oriented along the axis of the optic nerve, a recent comprehensive study of the ONH glial and connective tissue architecture has shown that a 3D glial network is present throughout the prelaminar, laminar, and retrolaminar optic nerve and that there is significant lateral connectivity between the retrolaminar septae.[39] These findings suggest that the LC can be viewed as simply a portion of the larger 3D glial structure that has synthesized the additional connective tissue components necessary to bear the forces of IOP within the scleral canal. Hence, transformation of the immediate retrolaminar septa into a horizontally oriented, lamina-like connective tissue architecture (recruitment into the load-bearing LC) through connective tissue synthesis seems plausible.

Biomechanically, such a recruitment scenario might unfold as follows: as the normal LC connective tissue becomes mechanically compromised because of chronically elevated IOP, an effect that may initially manifest as hypercompliance of the lamina cribrosa itself,[7] additional load and strain are borne by the immediate retrolaminar septa. The resident cell population in the newly stressed region then becomes activated through mechanotransduction[40–42] and reacts to restore the homeostatic stress and strain milieu in the LC structure through extracellular matrix remodeling.[6,43] Thus, the immediate retrolaminar septae (previously protected from large strains by the LC just anterior) remodel by synthesizing new connective tissue consistent with the 3D load-bearing LC structure. This reaction, occurring simultaneously with similar processes within the LC, would result in a thicker overall laminar structure[10] composed of more laminar beams (some of which may be thicker) and a larger nonconnective tissue volume (swollen axons and more glia).

Hayreh et al.[44] have reported retrolaminar fibrosis in the monkey model of EG in a qualitative 2D histologic study and suggested that this fibrosis and its subsequent contraction were primarily responsible for posterior deformation of the lamina seen in EG damage. Although our data do not elucidate the process by which the LC is posteriorly deformed, we believe this deformation is directly IOP related and that the remodeling of the retrolaminar septae is a result of IOP-related damage and deformation of the LC connective tissues, not the cause of it. The retrolaminar fibrosis that Hayreh et al.[44] observed is compatible with our hypothesis of thickening and recruitment of retrolaminar septae into the load-bearing LC structure, though the animals in their study had a more advanced stage of glaucomatous damage in which retrolaminar fibrosis could be expected on the basis of profound axon loss alone.

The results and conclusions of this report should be viewed with the following limitations in mind. First, the EG monkey ONHs were reconstructed at a different voxel resolution ($2.5 \times 2.5 \times 3.0$ μm) that was coarser than those of the bilaterally normal monkeys ($1.5 \times 1.5 \times 1.5$ μm). Second, the EG monkeys were all cynomolgus, and the normal monkeys were all rhesus. Either of these factors, or a combination of the two, could result in the systematic differences in the CTVF and anisotropy ratio between the groups seen in Figures 8 and 9. However, all the conclusions drawn herein are based on comparisons between contralateral eyes of the same monkey (both treated identically) or between monkeys in the same group (treated identically and of the same species) and so should not be affected by these limitations. Third, the coarseness of our finite element-based sampling scheme (necessary to have a sufficient number of laminar beams within each sampled subvolume to make the MIL measurements) may mask more subtle spatial patterns in LC connective tissue distribution. This issue will be explored in future reports using more continuous mapping schemes. Last, our staining and serial sectioning-based 3D reconstruction technique cannot distinguish between old, newly synthesized, and edematous connective tissue and does not stain nonconnective tissue, which makes it impossible to directly determine the sources of connective and nonconnective tissue volume increases in EG reported here. Additional work is needed to characterize regional alterations in beam thickness, number, and connectivity within the LC. These methods are under active development within our group and will be the subject of a future report.

In summary, the results presented here suggest a potent connective tissue remodeling response in the LC in the early stages of glaucomatous damage. The effect of this response is to dramatically increase the amount of LC connective tissue in the EG eyes while preserving the proportion of connective to nonconnective tissue (CTVF). The character of the LC microarchitecture (CTVF, predominant beam orientation, and anisotropy) is not significantly affected by the glaucomatous remodeling response. The maps of laminar CTVF, orientation, and anisotropy presented herein are useful for characterizing regional variations in structural parameters in normal eyes and changes that occur in EG. In addition, these data can be used to define regional material property descriptions (e.g., structural stiffness) of the LC for use in biomechanical models to relate changes in IOP to tissue-level displacement, stress, and strain in the ONH. The implementation of such a modeling approach will be the subject of future reports.

Acknowledgments

The authors thank Budd Hirons and Pris Zhou for their contributions to this work, and Ian Sigal for his careful reading of an early draft of the manuscript and for his assistance with figure generation.

References

1. Bellezza AJ, Hart RT, Burgoyne CF. The optic nerve head as a biomechanical structure: initial finite element modeling. *Invest Ophthalmol Vis Sci.* 2000;41:2991–3000.
2. Burgoyne CF, Downs JC, Bellezza AJ, Suh JK, Hart RT. The optic nerve head as a biomechanical structure: a new paradigm for understanding the role of IOP-related stress and strain in the pathophysiology of glaucomatous optic nerve head damage. *Prog Retin Eye Res.* 2005;24:39–73.
3. Minckler DS, Spaeth GL. Optic nerve damage in glaucoma. *Surv Ophthalmol.* 1981;26:128–148.
4. Hayreh SS. Blood supply of the optic nerve head and its role in optic atrophy, glaucoma, and oedema of the optic disc. *Br J Ophthalmol.* 1969;53:721–748.
5. Fechtner RD, Weinreb RN. Mechanisms of optic nerve damage in primary open angle glaucoma. *Surv Ophthalmol.* 1994;39:23–42.
6. Hernandez MR. The optic nerve head in glaucoma: role of astrocytes in tissue remodeling. *Prog Retin Eye Res.* 2000;19:297–321.
7. Bellezza AJ, Rintalan CJ, Thompson HW, Downs JC, Hart RT, Burgoyne CF. Deformation of the lamina cribrosa and anterior scleral canal wall in early experimental glaucoma. *Invest Ophthalmol Vis Sci.* 2003;44:623–637.
8. Downs JC, Yang H, Girkin C, et al. Three-dimensional histomorphometry of the normal and early glaucomatous monkey optic nerve head: neural canal and subarachnoid space architecture. *Invest Ophthalmol Vis Sci.* 2007;48:3195–3208.
9. Yang H, Downs JC, Bellezza AJ, Thompson H, Burgoyne CF. 3-D histomorphometry of the normal and early glaucomatous monkey optic nerve head: prelaminar neural tissues and cupping. *Invest Ophthalmol Vis Sci.* 2007;48:5068–5084.
10. Yang H, Downs JC, Girkin C, et al. 3-D histomorphometry of the normal and early glaucomatous monkey optic nerve head: lamina cribrosa and peripapillary scleral position and thickness. *Invest Ophthalmol Vis Sci.* 2007;48:4597–4607.
11. Quigley HA, Addicks EM. Regional differences in the structure of the lamina cribrosa and their relation to glaucomatous optic nerve damage. *Arch Ophthalmol.* 1981;99:137–143.
12. Dandona L, Quigley HA, Brown AE, Enger C. Quantitative regional structure of the normal human lamina cribrosa: a racial comparison. *Arch Ophthalmol.* 1990;108:393–398.
13. Radius RL. Regional specificity in anatomy at the lamina cribrosa. *Arch Ophthalmol.* 1981;99:478–480.
14. Ketcham RA, Ryan TM. Quantification and visualization of anisotropy in trabecular bone. *J Microsc.* 2004;213:158–171.
15. Odgaard A, Kabel J, van Rietbergen B, Dalstra M, Huiskes R. Fabric and elastic principal directions of cancellous bone are closely related. *J Biomech.* 1997;30:487–495.
16. Turner CH. On Wolff's law of trabecular architecture. *J Biomech.* 1992;25:1–9.
17. Oda M. A method for evaluating the effect of crack geometry on the mechanical behavior of cracked rock masses. *Mech Materials.* 1983;3:163–171.
18. Burgoyne CF, Downs JC, Bellezza AJ, Hart RT. Three-dimensional reconstruction of normal and early glaucoma monkey optic nerve head connective tissues. *Invest Ophthalmol Vis Sci.* 2004;45:4388–4399.
19. Grau V, Downs JC, Burgoyne CF. Segmentation of trabeculated structures using an anisotropic Markov random field: application to the study of the optic nerve head in glaucoma. *IEEE Trans Med Imaging.* 2006;25:245–255.
20. Hughes T. *The Finite Element Method*. Englewood Cliffs, NJ: Prentice-Hall; 1987.
21. Harrigan TP, Jasty M, Mann RW, Harris WH. Limitations of the continuum assumption in cancellous bone. *J Biomech.* 1988;21:269–275.
22. Cowin SC. Wolff's law of trabecular architecture at remodeling equilibrium. *J Biomech Eng.* 1986;108:83–88.
23. Turner CH, Cowin SC, Rho JY, Ashman RB, Rice JC. The fabric dependence of the orthotropic elastic constants of cancellous bone. *J Biomech.* 1990;23:549–561.
24. Harrigan TP, Mann RW. Characterization of microstructural anisotropy in orthotropic materials using a second rank tensor. *J Materials Sci.* 1984;19:761–767.
25. Yang H, Downs JC, Burgoyne CF. Physiologic intereye differences in monkey optic nerve head architecture and their relation to changes in early experimental glaucoma. *Invest Ophthalmol Vis Sci.* 2009;50:224–234.
26. Jonas JB, Berenshtein E, Holbach L. Anatomic relationship between lamina cribrosa, intraocular space, and cerebrospinal fluid space. *Invest Ophthalmol Vis Sci.* 2003;44:5189–5195.
27. Quigley HA, Addicks EM, Green WR, Maumenee AE. Optic nerve damage in human glaucoma, II: the site of injury and susceptibility to damage. *Arch Ophthalmol.* 1981;99:635–649.
28. Quigley HA, Hohman RM, Addicks EM, Massof RW, Green WR. Morphologic changes in the lamina cribrosa correlated with neural loss in open-angle glaucoma. *Am J Ophthalmol.* 1983;95:673–691.
29. Ogden TE, Duggan J, Danley K, Wilcox M, Minckler DS. Morphometry of nerve fiber bundle pores in the optic nerve head of the human. *Exp Eye Res.* 1988;46:559–568.
30. Jonas JB, Mardin CY, Schlotzer-Schrehardt U, Naumann GO. Morphometry of the human lamina cribrosa surface. *Invest Ophthalmol Vis Sci.* 1991;32:401–405.
31. Radius RL, Gonzales M. Anatomy of the lamina cribrosa in human eyes. *Arch Ophthalmol.* 1981;99:2159–2162.
32. Brown DJ, Morishige N, Neekhra A, Minckler DS, Jester JV. Application of second harmonic imaging microscopy to assess structural changes in optic nerve head structure ex vivo. *J Biomed Opt.* 2007;12:24–29.
33. Minckler DS. Histology of optic nerve damage in ocular hypertension and early glaucoma. *Surv Ophthalmol.* 1989;(suppl):401–402; discussion 409–411.
34. Morrison JC, Dorman-Pease ME, Dunkelberger GR, Quigley HA. Optic nerve head extracellular matrix in primary optic atrophy and experimental glaucoma. *Arch Ophthalmol.* 1990;108:1020–1024.
35. Hernandez MR, Ye H. Glaucoma: changes in extracellular matrix in the optic nerve head. *Ann Med.* 1993;25:309–315.
36. Hernandez MR, Ye H, Roy S. Collagen type IV gene expression in human optic nerve heads with primary open angle glaucoma. *Exp Eye Res.* 1994;59:41–51.
37. Hernandez MR, Agapova OA, Yang P, Salvador-Silva M, Ricard CS, Aoi S. Differential gene expression in astrocytes from human normal and glaucomatous optic nerve head analyzed by cDNA microarray. *Glia.* 2002;38:45–64.
38. Morrison JC, Johnson EC, Cepurna W, Jia L. Understanding mechanisms of pressure-induced optic nerve damage. *Prog Retin Eye Res.* 2005;24:217–240.
39. Oyama T, Abe H, Ushiki T. The connective tissue and glial framework in the optic nerve head of the normal human eye: light and

scanning electron microscopic studies. *Arch Histol Cytol.* 2006; 69:341–356.

40. Morrison JC. Integrins in the optic nerve head: potential roles in glaucomatous optic neuropathy (an American Ophthalmological Society thesis). *Trans Am Ophthalmol Soc*. 2006;104:453–477.
41. Kirwan RP, Crean JK, Fenerty CH, Clark AF, O'Brien CJ. Effect of cyclical mechanical stretch and exogenous transforming growth factor-beta1 on matrix metalloproteinase-2 activity in lamina cribrosa cells from the human optic nerve head. *J Glaucoma.* 2004; 13:327–334.
42. Kirwan RP, Fenerty CH, Crean J, Wordinger RJ, Clark AF, O'Brien CJ. Influence of cyclical mechanical strain on extracellular matrix gene expression in human lamina cribrosa cells in vitro. *Mol Vis.* 2005;11:798–810.
43. Hernandez MR, Andrzejewska WM, Neufeld AH. Changes in the extracellular matrix of the human optic nerve head in primary open-angle glaucoma. *Am J Ophthalmol.* 1990;109:180–188.
44. Hayreh SS, Pe'er J, Zimmerman MB. Morphologic changes in chronic high-pressure experimental glaucoma in rhesus monkeys. *J Glaucoma.* 1999;8:56–71.